

# Star Formation and AGN Activity in Interacting Galaxies: A Near-UV Perspective

Caroline Scott<sup>1,2,3\*</sup> and Sugata Kaviraj<sup>4,5,1</sup>

<sup>1</sup>*Astrophysics, Imperial College London, Blackett Laboratory, London SW7 2AZ, UK*

<sup>2</sup>*Harvard-Smithsonian Center for Astrophysics, 60 Garden Street, Cambridge, MA 02138, USA*

<sup>3</sup>*Institute for Applied Computational Science, Harvard University, 29 Oxford Street, Cambridge, MA 02138, USA*

<sup>4</sup>*Centre for Astrophysics Research, University of Hertfordshire, College Lane, Hatfield, Herts, AL10 9AB, UK*

<sup>5</sup>*Department of Physics, University of Oxford, Keble Road, Oxford, OX1 3RH, UK*

Accepted 18 October 2013

## ABSTRACT

We study nearby galaxies in close pairs to study the key factors affecting star formation and AGN activity triggered during galaxy interactions. Close pairs are selected from the Sloan Digital Sky Survey assuming a projected separation of  $<30$  kpc and recession velocity difference  $<500$  km s<sup>-1</sup>. Near-ultraviolet (NUV) fluxes from GALEX are used to estimate specific star formation rates (SSFRs). We find a factor of  $\sim 5.3$  increase in SSFR for low mass ( $10^8$ - $10^{11} M_{\odot}$ ) close pair galaxies and a factor of  $\sim 2.1$  increase in SSFR for high mass ( $10^{11}$ - $10^{13} M_{\odot}$ ) close pairs compared to the general galaxy population. Considering galaxies of all masses, we find a factor of  $\sim 1.8$  enhancement in SSFR for close pairs in field environments compared to non-pairs, with no significant increase for pairs in group and cluster environments. A modest decrease of a factor of  $\sim 1.4$  is found in the Seyfert fraction in close pair galaxies when compared to isolated galaxies, which suggests that mergers may not trigger AGN activity at the close-pair stage or may trigger a different class of AGN. This becomes a factor of  $\sim 4.2$  decrease when we restrict our analysis to high mass close pairs in group or cluster environments.

**Key words:** galaxies: formation - galaxies: evolution - galaxies: interactions - galaxies: star formation - galaxies: active

## 1 INTRODUCTION

Mergers are fundamental to the standard hierarchical paradigm of galaxy formation and evolution. Models predict that they produce intense star formation episodes (Mihos & Hernquist 1996; Cox et al. 2008; Bournaud et al. 2011), contributing to the build-up of stellar mass and black holes (Sanders & Mirabel 1996; Hopkins et al. 2005; Debuhr et al. 2011), and alter the morphological mix of the Universe (Toomre & Toomre 1972; Kauffmann et al. 1993; Mihos 1995; Kauffmann & Haehnelt 2000). Past studies from the previous generation of astrophysical instruments found that interactions could enhance star formation in close pair galaxies (Larson & Tinsley 1978; Joseph et al. 1984; Lonsdale et al. 1984) and potentially trigger AGN activity (Smith et al. 1986; Hutchings 1987; Sanders et al. 1988). Since the emergence of large-scale galaxy surveys, such as the Sloan Digital Sky Survey (SDSS) and the Galaxy Evo-

lution Explorer (GALEX), robust statistical analyses can now be conducted on galaxy-galaxy interactions, resulting in extensive studies of mergers over recent years.

Substantial observational data now serves to complement results from simulations, which claim that close pair interactions and mergers cause the instability needed for gas clouds to collapse and produce starbursts (e.g. Kauffmann & Haehnelt 2000). Spectroscopic and photometric evidence from large scale surveys such as IRAS (Kennicutt et al. 1987) and the SDSS (Ellison et al. 2008), and high resolution instruments like the HST (Patton et al. 2005) have bolstered such claims. Morphological asymmetry effects are also a trade mark signature of close pair systems; with most of the galaxies in the Arp catalogue (Atlas of Peculiar Galaxies, Arp 1966) showing signs of recent tidal interactions (Larson & Tinsley 1978) and  $\sim 40\%$  of close pair systems expected to show asymmetry effects (Patton et al. 2005). Interaction-induced effects are expected to depend on properties of the progenitor galaxies and external pair-properties of close pair systems. Such properties may include

\* email cscott@cfa.harvard.edu

the environment in which the merger is taking place, pair separation, the type of galaxies merging (e.g. morphology, mass), and central galactic processes within the progenitors; such as feedback from AGN activity.

Close pair systems which are in the early stages of merging generally show less resulting star formation than further advanced mergers (e.g. Larson & Tinsley 1978; Barton et al. 2000). Using H $\alpha$  as a diagnostic for star formation for a large sample of spectroscopically classified SDSS DR5 close pairs, Woods & Geller (2007) found evidence that the lower mass progenitor in a minor merger will experience the most star formation. Ellison et al. (2008) found an enhancement in star formation in close pairs of up to 70% compared with a control sample of 40,095 SDSS galaxies which had the same mass distribution. This enhancement in star formation was greatest for major mergers; where the progenitors have mass ratio  $M_1/M_2 > 0.5$ . Wong et al. (2011) used UV photometry from GALEX to look at NUV-r and FUV-r colours for intermediate redshift close pairs ( $0.25 \leq z \leq 0.75$ ) drawn from the Prism Multi-Object Survey (PRIMUS). They find an  $\sim 15-20\%$  increase in SSFR for close pairs with projected separation  $\leq 50h^{-1}$  kpc, and an  $\sim 25-30\%$  increase in SSFR for close pairs with projected separation  $\leq 30h^{-1}$  kpc.

Dense environments, such as galaxy clusters, often have lower gas fractions as a result of tidal fields and ram pressure stripping (Byrd & Valtonen 1990); as a consequence, less gas is thought to be available to fuel star formation during a merger. Accordingly, close pairs in galaxy clusters and groups have been found to show comparatively less star formation than close pairs in the field (Kauffmann et al. 2004; Alonso et al. 2005; Ellison et al. 2010). Using SDSS DR4 data, Ellison et al. (2010) found a decrease in star formation in local dense environments when using asymmetry and optical colours to indicate interaction-induced star formation. They concluded that the higher levels of star formation detected in close pairs in low density environments is a result of the higher gas fraction available to fuel star formation.

Studies of radio and QSO galaxies found that a significant number of radio galaxies are currently interacting or show recent signs of merger activity (e.g. Smith et al. 1986; Hutchings 1987); suggesting a link between close pair galaxies and AGN activity. Hutchings (1987) noted that AGN activity is generally observed in the larger of two interacting galaxies and suggested that in minor mergers the smaller galaxy can serve to fuel nuclear activity in the massive (often elliptical) galaxy.

Since recently formed stars ( $\lesssim 1$ Gyr) are responsible for most of a galaxy's UV luminosity, recent star formation rates strongly correlate with UV luminosity (Iglesias-Páramo et al. 2006). Salim et al. (2005) show that NUV-r colour alone is sufficient to estimate the star formation history of galaxies and that GALEX is sensitive to star formation levels as low as  $\sim 10^{-3} M_{\odot} \text{ yr}^{-1}$ . GALEX's NUV band (effective wavelength: 2271Å) allows us to study star formation with much more sensitivity to recent star formation than optical filters (Yi et al. 2005; Kaviraj et al. 2007; Donas et al. 2007; Bianchi 2011).

Emission line tracers of star formation (e.g. H $\alpha$ ) often limit measurements to the central galactic regions due to finite fibre size. SDSS fibres have a size of  $3''$  and therefore they measure a different fraction of light in each galaxy. Even though corrections can be made based on the ratio

of the Petrosian-to-fibre flux, this correction is somewhat uncertain (e.g. Brinchmann et al. 2004). However, UV photometry provides a measure of emission from young stars for the full extent of a galaxy. One caveat is the NUV band is extremely sensitive to interstellar reddening, more-so than optical and IR photometry (Meurer et al. 1999; Pannella et al. 2009). We correct our GALEX flux measurements for interstellar extinction using the Balmer decrement from the SDSS spectrum.

In this work recent star formation is examined in close pair galaxies at various stages of the merger process. Properties such as mass, close pair (projected) separation, environment and AGN activity are investigated to see how they affect star formation in pairs; where possible we try to break degeneracies between these properties. This work offers a similar investigation to some previous research, but from an optical-UV perspective and with a broad range of derived properties to investigate close pairs with various characteristics in detail.

In Section 2 we describe how the close pairs and wide pairs samples were extracted from the SDSS database, the process by which these samples were cross-matched with GALEX data and how the properties for our study (such as mass, environment, BPT classification etc.) were derived. In Section 3 we present the results of our analysis. In Section 4 we look at the fraction of Transition, LINER and Seyfert galaxies in projected separation bins from 0-150kpc to investigate potential changes to these fractions as merging galaxies draw closer together. The evolution of these fractions with decreasing projected separation is studied as a function of mass and environment. In Section 5 the results are summarised and discussed.

## 2 SAMPLE DESCRIPTION

### 2.1 SDSS and GALEX

Our close pairs catalogue is extracted from the SDSS Data Release 7 (DR7) database (Fukugita et al. 1996; Gunn et al. 1998; York et al. 2000). The SDSS uses a multi-object fibre spectrograph to observe spectra over an area of  $\sim 10,000 \text{ deg}^2$ . Photometric data is imaged using five optical filters  $u, g, r, i, z$  over a 3,000-11,000Å range (where 3,000Å is the atmospheric UV cut-off wavelength and 11,000Å is the silicon sensitivity limit of the CCDs) using a large format mosaic CCD camera. Spectra for objects within  $55''$  can only be obtained if they are observed in overlapping tiles. These so-called *fibre collisions* present an incompleteness issue when studying galaxy close pairs as only  $\sim 30\%$  of the  $10,000 \text{ deg}^2$  area covered by the SDSS is observed by overlapping tiles (Darg et al. 2010). However, since the pairs that are detected are drawn randomly from a homogenous sample, our catalogue constitutes a representative (yet incomplete) sample of low redshift close pairs.

GALEX (Galaxy Evolution Explorer) is a NASA space based all-sky survey observing at ultraviolet wavelengths with  $4-6''$  resolution and  $\sim 50 \text{ cm}^2$  effective area (Morrissey et al. 2007). GALEX images in  $1.2$  diameter circular fields at 1770-2730Å (NUV) and 1350-1780Å (FUV) simultaneously, using a modified Ritchey Chrétien telescope. The FUV limit is 5000 cts/s,  $m_{AB} = 9.5$ ,  $F_{\lambda} = 7 \times 10^{-12} \text{ erg}$

$\text{cm}^{-2} \text{s}^{-1} \text{\AA}^{-1}$  and the NUV limit is 30,000 cts/s,  $m_{AB} = 8.9$ ,  $F_{\lambda} = 6 \times 10^{-12} \text{ erg cm}^{-2} \text{s}^{-1} \text{\AA}^{-1}$ .

We use the GR4/GR5 database which combines data from the following imaging surveys: All-sky Imaging Survey (AIS), Deep Imaging Survey (DIS), Medium Imaging Survey (MIS), Nearby Galaxy Survey (NGS) (Martin et al. 2005; Morrissey et al. 2005). Our sample is mainly from the AIS and MIS surveys. The AIS has 100s exposure time,  $26,000 \text{deg}^2$  sky coverage,  $m_{AB} = 20.5$  depth and 28,000 tiles. The MIS has 1,500s exposure time,  $1,000 \text{deg}^2$  sky coverage,  $m_{AB} = 23.5$  depth and 1615 tiles. AIS covers around 3/4 of the sky and aims to provide an all-sky survey with similar depth to the Palomar Observatory Sky Survey II and the SDSS. Regions in the vicinity of the Galactic plane and the Magellanic clouds were avoided due to the sensitivity of detectors in order to safeguard the detectors from potentially over-saturating UV fluxes. As a result, imaging in the surrounding areas can be patchy, but otherwise fields are generally adjacent. MIS is also positioned to have a significant overlap with the SDSS; there is a  $7325 \text{deg}^2$  overlap between SDSS DR7 and AIS (GR5) and  $1103 \text{deg}^2$  with the MIS (GR5) (Bianchi 2011).

## 2.2 Pair Extraction and Cross-Matching

To extract close pairs from the SDSS DR7 database we use a procedure to seek galaxies with small angular separation and a small recessional velocity difference (i.e. low separation in the line-of-sight direction). We follow Patton et al. (2002) who suggest a projected separation of  $20h^{-1} \text{kpc}$  and a difference in recessional velocities of  $500 \text{km s}^{-1}$ . Soares (2007) compares projected separation with spatial separation for a Monte Carlo simulated sample of gravitationally-bound pairs and finds that over 50% with projected separation  $\leq 50 \text{kpc}$  actually have spatial separation  $> 50 \text{kpc}$ . Thus, we accept that projected separation is merely an approximation to spatial separation, and that the physical separation is likely to be higher. Incompleteness due to fibre collisions, large peculiar velocities, minor mergers (low mass galaxies are often below the SDSS spectroscopic limit of  $r < 17.77$ ) etc. result in only  $\sim 30\%$  of close pairs being detected. Since the sample used is from a low redshift survey and is magnitude limited, we do not impose a maximum redshift constraint. We remove all systems where more than one SDSS object (including the primary object) is within  $5''$  of a GALEX object ( $5''$  being the GALEX resolution). The median redshift is  $z \sim 0.07$ . The close pairs sample consists of 6668 galaxies with SDSS data and 2902 galaxies with both SDSS and NUV photometry. A *wide pairs* sample with projected separation 30-150kpc and  $\Delta z \sim 0.0017$  was also extracted to be used as a control sample with which to compare the close pairs sample. The wide pairs sample consists of 34,294 galaxies with SDSS data and 19,202 galaxies with both SDSS and NUV data.

Kcorrect V4.2 (Blanton & Roweis 2007) was used to calculate K-corrections for the (galactic extinction-corrected) SDSS/GALEX apparent magnitudes, then absolute magnitudes were derived. Stellar masses were approximated using the following formula from Wang et al. (2006)

(based on Bell et al. 2003);

$$\log(M_*/M_{\odot}) = -0.4[\text{Mag}(r) - 4.67] - 0.306 + 1.097[\text{Mag}(g) - \text{Mag}(r)] + 0.15, \quad (1)$$

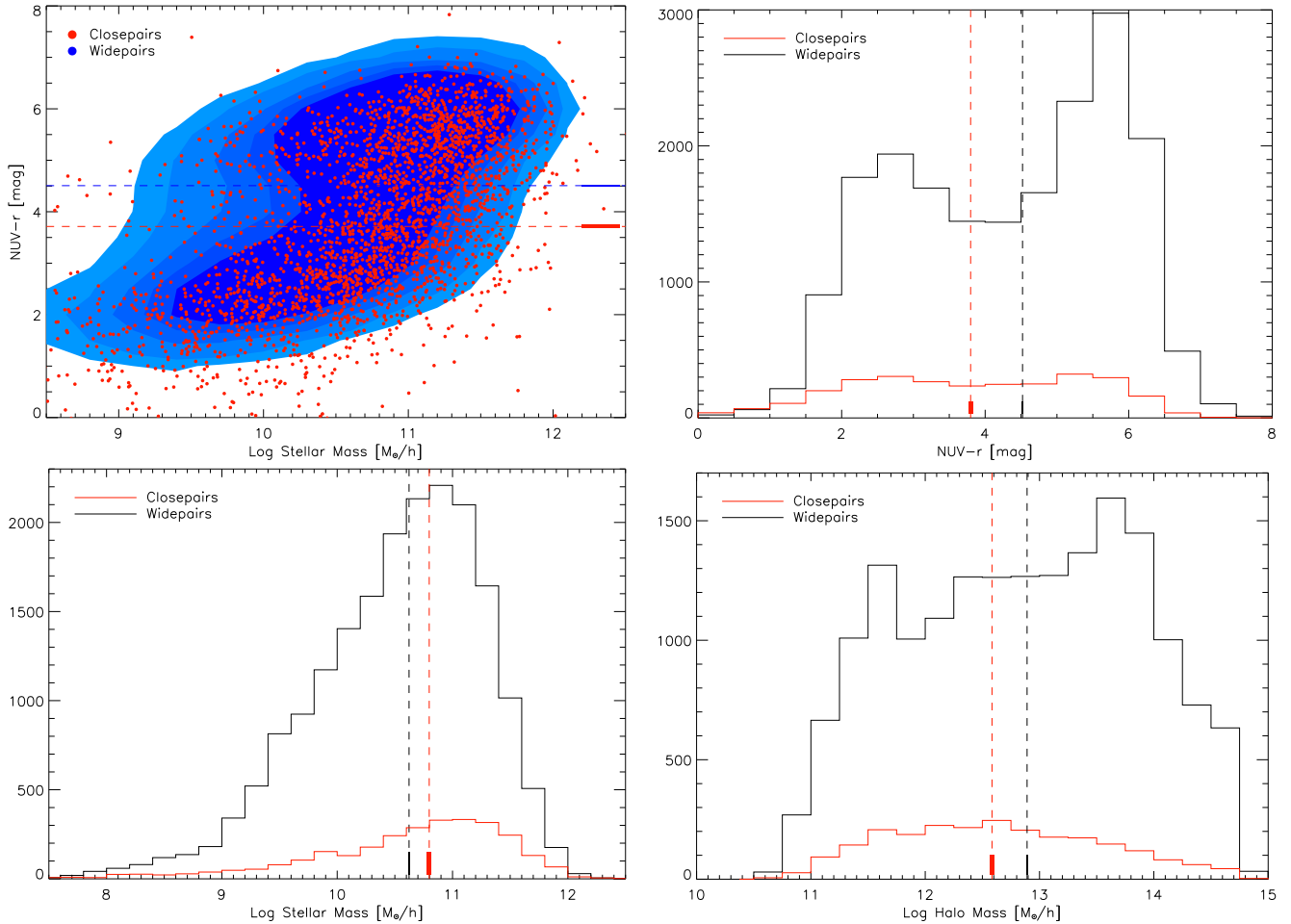
where 4.67 is the  $r$ -band solar absolute magnitude from the SDSS. This assumes a Salpeter (1955) stellar IMF with  $dN/dM \propto M^{-2.35}$  and  $0.1M_{\odot} < M < 100M_{\odot}$ . The median uncertainty in stellar mass values is  $\sim 0.1$  dex, with maximum uncertainty expected to be  $\sim 0.2$  dex.

Figure 1 (top) shows the NUV- $r$  distribution for the close and wide pairs samples. The bottom left histogram shows the stellar mass distribution; the close pairs sample has a median stellar mass of  $10^{10.8} M_{\odot}$  and the wide pairs sample has a slightly lower median stellar mass of  $10^{10.6} M_{\odot}$ . Bundy et al. (2009) and Darg et al. (2010) find a similar bias towards higher stellar masses (by  $\sim 0.2$  dex) for close pairs. This was suggested to be a result of the increased merger fraction in higher density environments, where massive red spheroidal galaxies are more common. However, Simard et al. (2011) show that photometry for close pairs from the standard SDSS pipeline is sometimes poor for pairs with projected separation  $\lesssim 20 \text{kpc}$  and Patton et al. (2011) suggest that this has led some authors to incorrectly perceive an extremely red population in close pairs samples. This reddening effect would explain our bias towards higher stellar masses for the close pairs, however, since the difference lies within the stellar mass error we justify their use.

## 2.3 Environment and Emission-Line Analysis

The close and wide pairs samples were crossmatched with an environment catalogue derived from a halo-based group finder (Yang et al. 2005, 2007). This method primarily uses the friends-of-friends algorithm to find groups (Huchra & Geller 1982), then approximates the group centre using its brightest member. An initial mass is calculated using the mass-to-light ratio, then the total luminosity of potential groups is estimated using the luminosity function from Norberg et al. (2002). All galaxies are then assigned a probability of belonging to each group's dark matter halo. The algorithm iteratively assigns each galaxy to its most probable group (merging smaller groups that can be identified as one), updates the assigned group centre, and recalculates the total luminosity. The dark matter halo mass is then calculated from this finalised characteristic luminosity, and is used to approximate environment density. Figure 1 (bottom right) shows the distribution of the halo mass parameter for both samples. We assume that a halo mass value from  $10^{10}$  to  $10^{13} M_{\odot}$  describes a local field environment,  $10^{13}$  to  $10^{14} M_{\odot}$  a group environment, and  $10^{14}$  to  $10^{15} M_{\odot}$  a cluster environment (Kaviraj et al. 2009).

A BPT analysis (Baldwin et al. 1981; Kewley et al. 2001; Kauffmann et al. 2003; Kewley et al. 2006; Trichas et al. 2010; Kalfountzou et al. 2011) allows us to determine the predominant mechanism of excitation in our sample galaxies. Intensity ratios of pairs of strong emission lines are used to separate Starburst galaxies from AGN. In Figure 2, we plot  $\log([\text{NII}]/\text{H}\alpha)$  against  $\log([\text{OIII}]/\text{H}\beta)$  and classify each galaxy as Starburst, Transition, LINER or Seyfert depending on where they lie on the BPT diagram; as defined by Kauffmann et al. (2003). A



**Figure 1.** Top: NUV-*r* against stellar mass plot (left) and histogram (right) for the wide pairs (black) and close pairs (red) samples. Bottom: stellar mass distribution (left) and halo mass distribution (right) for the wide and close pairs samples. Dotted lines represent median values, and coloured blocks on median lines show bootstrapping results.

Quiescent class is defined, though very few of our galaxies lie in the Quiescent region. Type I (i.e. unobscured) AGN are flagged and removed before the analysis. We consider LINER and Seyfert galaxies as Type II AGN. Only galaxies with [NII] and H $\alpha$  emission line signal-to-noise ratio >3 are used.

## 2.4 Deriving Star Formation Rates

We compute star formation rates (SFRs) for galaxies in our sample from their NUV absolute magnitudes using the following expression from Iglesias-Páramo et al. (2006):

$$\log \text{SFR}_{\text{NUV}} (M_{\odot} \text{yr}^{-1}) = \log L_{\text{NUV}} (L_{\odot}) - 9.33 \quad (2)$$

NUV fluxes were first corrected for internal reddening in the galaxy via the Balmer decrement, measured using the Gas and Absorption Line Fitting code (GANDALF; Sarzi et al. (2006)). GANDALF fits stellar population and emission line templates to the galaxy spectrum simultaneously, to separate the stellar continuum and absorption lines from the ionized gas emission. It calculates an internal E(B-V) from the emission lines, in the standard way, via the Balmer decrement assuming Case B recombination. This internal E(B-V)

likely traces the E(B-V) in the star-forming regions and is used to derive intrinsic NUV fluxes and star formation rates. To correct for internal and galactic extinction, we multiply the E(B-V) component by 2.751 (according to Schlegel et al. 1998) to correct our SDSS *r*-band magnitudes and by 8.2 (according to Calzetti et al. 2000; Kaviraj et al. 2007) to correct our GALEX NUV magnitudes.

We compare our NUV SFRs with those derived via H $\alpha$  fluxes in the MPA-JHU SDSS DR7 catalogues for the same galaxies<sup>1</sup>. These were derived from emission line luminosities (based on Brinchmann et al. 2004). Our wide pairs sample provides a suitable comparison between SFR measurements for the general galaxy population (see Figure 3). For the wide pairs, our NUV-derived SFRs have a slightly higher SFR distribution than the MPA emission line derived SFRs but overall show good agreement; whereas for close pairs the SFR is generally higher when measured using NUV luminosities. Note that the total emission line SFRs are calculated by scaling the H $\alpha$  flux by the ratio of the fibre and Petrosian fluxes. The reason for the discrepancy could lie in this scaling, which may not fully capture the age gradient in

<sup>1</sup> [www.mpa-garching.mpg.de/SDSS/DR7/](http://www.mpa-garching.mpg.de/SDSS/DR7/)

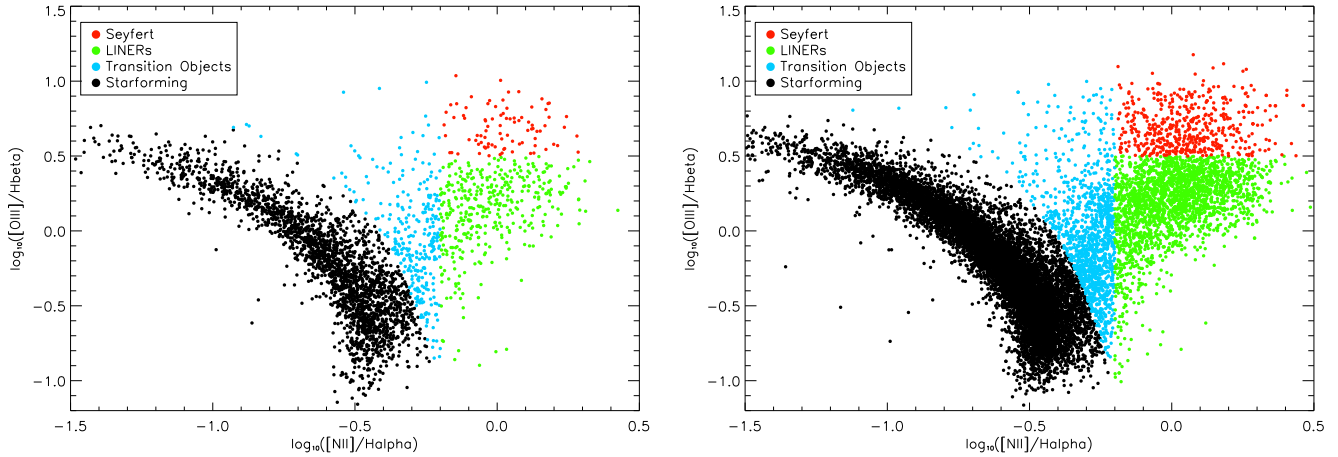


**Figure 2.** BPT:  $\log_{10}([\text{NII}]/\text{H}\alpha)$  is plotted against  $\log_{10}([\text{OIII}]/\text{H}\beta)$  for the close pairs (left) and wide pairs (right). Objects are classified as Starburst, Transition, LINER or Seyfert depending on the region they inhabit on the BPT diagram.

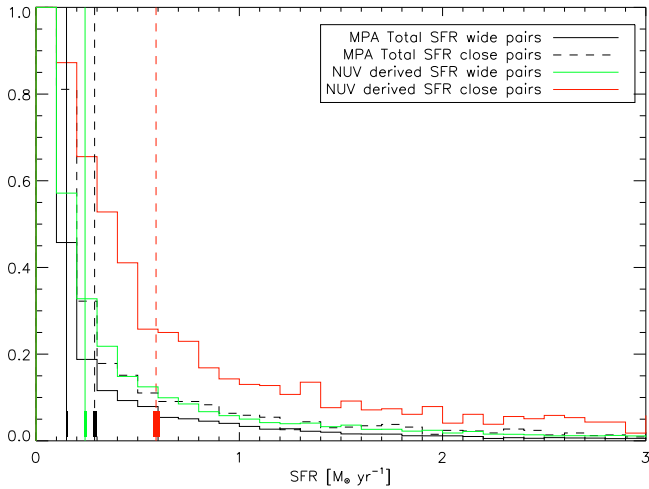


**Figure 3.** Emission line luminosity-derived SFRs from the MPA SDSS DR7 catalogue (black) are compared with NUV photometry-derived SFRs for our wide pairs sample (green) and close pairs sample (red). Vertical lines show sample median values.

the galaxy. We divide the NUV photometry-derived SFRs by the stellar mass attained from (1) for each galaxy to get specific star formation rates (SSFRs).

### 3 RESULTS

#### 3.1 Enhancement of Star Formation as a Function of Separation and Mass

In Figure 4 we split the close pairs and wide pairs samples into low stellar mass ( $10^8$ - $10^{11}M_{\odot}$ , shown in blue) and high stellar mass ( $10^{11}$ - $10^{13}M_{\odot}$ , shown in red) galaxies. To investigate the star formation enhancement in advancing mergers, both low mass and high mass galaxies are binned further by projected separation and we analyse median NUV- $r$  trends in these bins as separation decreases. For both stellar mass bins, the median NUV- $r$  colours become bluer as projected

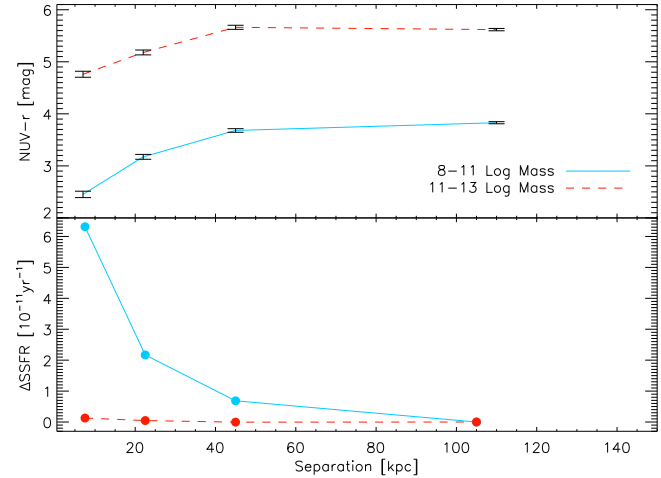


**Figure 4.** Top: Median NUV- $r$  colours for close and wide pairs binned by separation (0-15kpc, 15-30kpc, 30-60kpc and 90-130kpc) for both low stellar mass galaxies ( $10^8$ - $10^{11}M_{\odot}$ , shown in blue) and high stellar mass galaxies ( $10^{11}$ - $10^{13}M_{\odot}$ , shown in red). Bottom: SSFR difference between the separation bin in question and the widest separation bin, for both low and high mass galaxies. The fractional  $\Delta$ SSFR error is  $\sim 10\%$  for the low mass sample and  $\sim 30\%$  for the high mass sample.

separation decreases, indicating that recent star formation is enhanced as pairs draw closer together. This decrease occurs at approximately the same rate for the lower and the higher stellar mass bins.

In Table 1 we show the median SSFR ( $\text{yr}^{-1}$ ) for the galaxies in each mass/separation bin. We also plot the difference in SSFR between the widest separation bin and the separation bin in question (this quantity is by definition zero for the widest separation bin). We find a difference of  $6.3 \times 10^{-11} \text{yr}^{-1}$  in SSFR from the widest (90-130kpc) to the smallest separation bin (0-15kpc) for low stellar mass galaxies, and a difference of  $1.3 \times 10^{-12} \text{yr}^{-1}$  for high stellar mass galaxies. Treating the widest separation bin as a control sample, representative of the general population of non-close pair galaxies, this indicates a factor of 5.3 increase in SSFR for low stellar mass close pair galaxies and a fac-

Mass Range ( $\text{Log}_{10}M_{\odot}$ )	Projected Separation (kpc)			
	0-15	15-30	30-60	90-130
8-11	$8.24 \times 10^{-11}$	$3.77 \times 10^{-11}$	$2.63 \times 10^{-11}$	$1.94 \times 10^{-11}$
11-13	$3.22 \times 10^{-12}$	$1.98 \times 10^{-12}$	$1.22 \times 10^{-12}$	$1.31 \times 10^{-12}$

**Table 1.** Median SSFR ( $\text{yr}^{-1}$ ) derived from NUV luminosity for each stellar mass and separation bin.

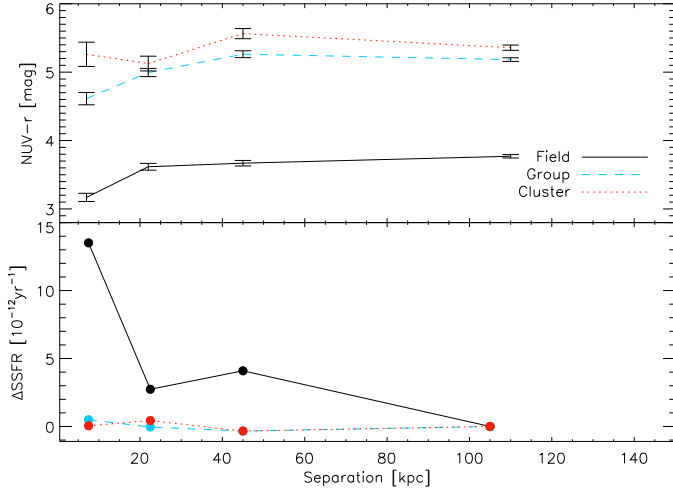


**Figure 5.** Top: Median NUV- $r$  colours for close and wide pairs binned by separation (0-15kpc, 15-30kpc, 30-60kpc and 90-130kpc) for pairs in field (black), group (blue) and cluster (red) environments. Bottom: SSFR difference between the separation bin in question and the widest separation bin, for each environment. The fractional  $\Delta$ SSFR error is  $\sim 20\%$ .

tor of 2.1 increase in SSFR for high stellar mass close pairs compared to the general galaxy population.

### 3.2 Enhancement of Star Formation as a Function of Separation and Environment

We now split the sample by environment and separation instead of stellar mass and separation. The three environment bins are field, group and cluster. We see in Figure 5 that the NUV- $r$  colour distribution shifts to bluer colours from the high density cluster environment to the low density field environment. As well as for general population galaxies in lower density environments, studies show strong evidence that particularly enhanced star formation takes place in close pairs in lower density environments (Kauffmann et al. 2004; Alonso et al. 2005; Ellison et al. 2010). We now quantify this from an NUV perspective.

We find a difference of  $1.4 \times 10^{-11} \text{yr}^{-1}$  (i.e. a factor of 1.8 increase) in SSFR from the widest to the smallest separation bin for pairs in field environments, and no significant increase for pairs in group and cluster environments. From our NUV perspective, this bolsters claims that decreasing local environment density leads to an increase in interaction-induced star formation for close pair galaxies which is greater than the enhancement expected for general population galaxies in low density environments.

Since stellar mass and environment are correlated, such that increasingly massive galaxies tend to be found in higher density environments, we attempt to break the degeneracy

by splitting our sample by stellar mass and environment. Figure 6 shows the environment/separation analysis, but now restricted to low mass galaxies ( $10^8$ - $10^{11}M_{\odot}$  -left) and higher mass galaxies ( $10^{11}$ - $10^{13}M_{\odot}$  -right). In the low mass analysis, NUV- $r$  colours in field and group environments become noticeably bluer with decreasing projected separation; with no clear trend for cluster environments. We find a rise in SSFR of  $4.4 \times 10^{-11} \text{yr}^{-1}$  (a factor of 2.4 increase) for field pairs and a rise of  $1.2 \times 10^{-11} \text{yr}^{-1}$  (a factor of 3.4 increase) for group pairs in the low mass sample. For high mass pairs the NUV- $r$  range is much narrower and lies in the redder colour region, implying that less recent star formation is being triggered. We see a rise of  $3.9 \times 10^{-12} \text{yr}^{-1}$  (a factor of 2.5 increase) in SSFR for high mass pairs in field environments.

## 4 AGN ACTIVITY IN CLOSE PAIRS

We wish to study how AGN activity evolves as a function of separation in close pairs. The BPT catalogue categorises the close and wide pairs samples into Starburst, Transition, LINER and Seyfert classifications. LINER galaxies can show similar line widths to the narrow-line region in Seyferts and are often difficult to distinguish between in the BPT diagram (Heckman 1980). We define a LINER/Seyfert class to represent galaxies that have  $\log([\text{NII}]/\text{H}\alpha) > -0.2$  but have [OIII] or  $\text{H}\beta$  lines with signal-to-noise  $\leq 3$  and so can not be classified distinctly between LINER and Seyfert. We analyse how the Transition, LINER, Seyfert and LINER/Seyfert fractions change as pairs advance to the lowest separation bin. Our aim is to see if the AGN fraction rises; i.e. if AGN activity is somehow ignited in some close pairs as the merging process advances. The pairs sample is split into four projected separation bins (0-15kpc, 15-30kpc, 30-80kpc and 80-150kpc).

Figure 7 (top left) shows the fraction of galaxies in each separation and BPT classification bin. Although we have restricted our analysis to not include Starburst and Quiescent galaxies, we include these in the total sample when calculating fractions. The error bars shown are standard Poisson number count errors. As pair separation decreases, the fraction in the LINER/Seyfert class decreases significantly and we see a steady rise in the Transition class. We see a drop in the Seyfert fraction from 5.9% (in the widest separation bin) to 4.3% (in the smallest separation bin); i.e. a factor of 1.4 drop. Since galaxies with stellar mass below  $\sim 10^{10}M_{\odot}$  are unlikely to host AGN (Kauffmann et al. 2003), we now restrict the analysis to higher stellar mass galaxies ( $M \geq 10^{10}M_{\odot}$ ); see the top right plot in Figure 7. This plot shows a similar distribution to the full stellar mass sample, but now each category accounts for a higher fraction. Here, we see a drop in the Seyfert fraction from 7.3% to 5.8%; a factor of 1.3 decrease.

We further split the sample into pairs in the field (Fig-

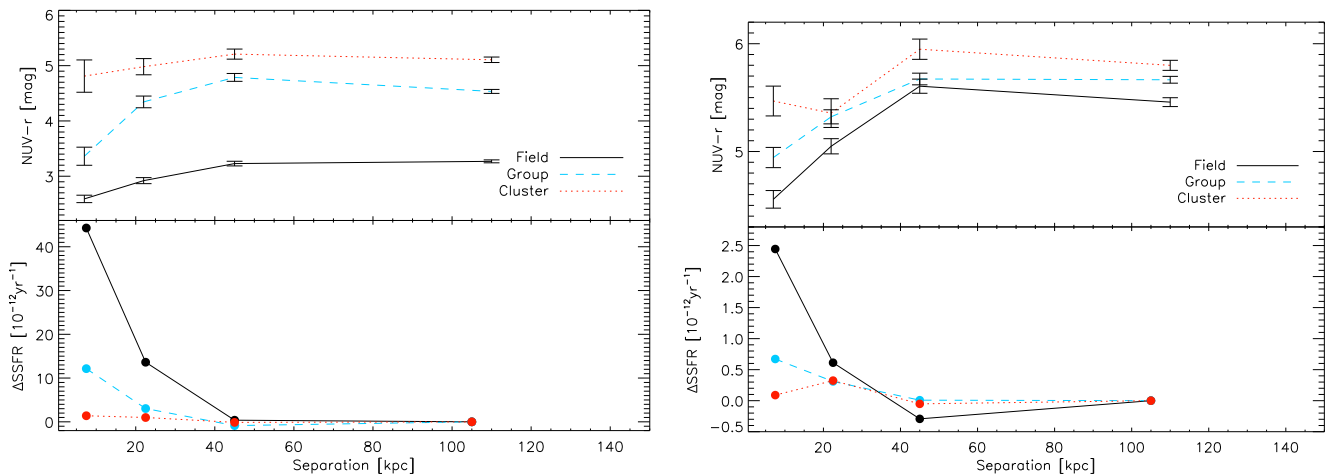


**Figure 6.** Median NUV- $r$  values for each environment/separation bin are plotted for low stellar mass galaxies ( $10^8$ - $10^{11}M_{\odot}$  -left) and high stellar mass galaxies ( $10^{11}$ - $10^{13}M_{\odot}$  -right).

ure 7 bottom left) and pairs in group/cluster environments (bottom right). In the field, we see no significant increase or decrease in the Seyfert fraction, however, we do see a rise in the Transition fraction for the closest pairs. In high density environment pairs we see a significant drop in the Seyfert fraction from 1.0% to 0.2%; a factor of 4.2 decrease. Note that after splitting by stellar mass and environment, we are left with few galaxies in the smallest separation Seyfert bins. Note also that the LINER and LINER/Seyfert fractions are equal in the final plot; both bins contain only 45 galaxies. We are generally seeing a small decrease in Seyfert fraction in pairs at very low separation, paralleled with an increase in the Transition fraction. This suggests that AGN activity may increase but it may be overwhelmed by star formation in low separation close pairs.

## 5 DISCUSSION AND SUMMARY

We study close pair galaxies using NUV- $r$  colours and NUV-derived specific star formation rates. This serves to add to previous work on close pairs in which optical colours and emission lines are used as indicators of star formation. Whereas emission line measurements are limited by finite fibre size and rely on corrections, NUV photometry provides a broader measure of young star formation for an entire galaxy. Our sample consists of SDSS optical spectroscopy and photometry, and GALEX photometry for low redshift close pair systems, and we also extract a sample of wide pair galaxies to use as a control sample representative of the general population.

We find a factor of 5.3 increase ( $6.3 \times 10^{-11} \text{yr}^{-1}$ ) in SSFR for low stellar mass close pair galaxies and a factor of 2.1 increase ( $1.3 \times 10^{-12} \text{yr}^{-1}$ ) in SSFR for high stellar mass close pairs compared to the general galaxy population. We find a difference of  $1.4 \times 10^{-11} \text{yr}^{-1}$  (i.e. a factor of 1.8 increase) in SSFR from the widest to the smallest separation bins for pairs in field environments, and no significant increase for pairs in group and cluster environments. In the low mass sample we find a rise in SSFR of  $4.4 \times 10^{-11} \text{yr}^{-1}$  (a factor of 2.4 increase) for pairs in the field and a rise of

$1.2 \times 10^{-11} \text{yr}^{-1}$  (a factor of 3.4 increase) for pairs in groups. For high mass pairs we see a rise of  $3.9 \times 10^{-12} \text{yr}^{-1}$  (a factor of 2.5 increase) in SSFR in field environments.

These results are consistent with Wong et al. (2011), who used NUV- $r$  and FUV- $r$  colours from GALEX as a proxy for SSFR for intermediate redshift close pairs ( $0.25 \leq z \leq 0.75$ ) drawn from PRIMUS. They found an  $\sim 15 - 20\%$  increase in SSFR for close pairs with projected separation  $\leq 50 h^{-1}$  kpc, and an  $\sim 25 - 30\%$  increase in SSFR for close pairs with projected separation  $\leq 30 h^{-1}$  kpc. PRIMUS spectra is lower resolution than SDSS spectra (redshifts are accurate to within  $\sigma_z/(1+z)$  with  $\lesssim 3\%$  catastrophic outliers), and the coverage is less ( $9.1 \text{ deg}^2$  of the sky, using multiple independent fields). Our SSFRs were calculated directly from the NUV luminosity, whereas Wong et al. use colours to estimate SSFR; yet despite different methods for estimating SSFR, the implications of enhancement in close pairs are consistent. A combination of these two studies shows evidence for SSFR enhancement from local to intermediate redshift close pairs.

Our results are also consistent with previous work on close pairs using optical colours and emission lines as tracers of star formation. Woods & Geller (2007) also find an enhancement in star formation in low mass galaxy close pairs using  $\text{H}\alpha$  as a diagnostic for star formation. Using asymmetry effects and optical colours as tracers, Kauffmann et al. (2004), Alonso et al. (2005) and Ellison et al. (2010) also find an enhancement in star formation in low density environments. This is likely to be due to the higher gas fraction available in low density environments to fuel star formation, since tidal fields and ram pressure stripping can lower gas fractions in higher density environments.

We find a significant drop in the Seyfert fraction as interactions progress to the nearly coalesced stage. For all masses and environments, we see a factor of 1.4 decrease in Seyfert fraction from general population galaxies to close pairs. This is particularly prominent in high mass close pairs in group environments, where we find a factor of 4.2 decrease in Seyfert fraction. A steady rise is also seen in the fraction of galaxies in the Transition region of the BPT diagram.

We see strong evidence that merging can cause a change

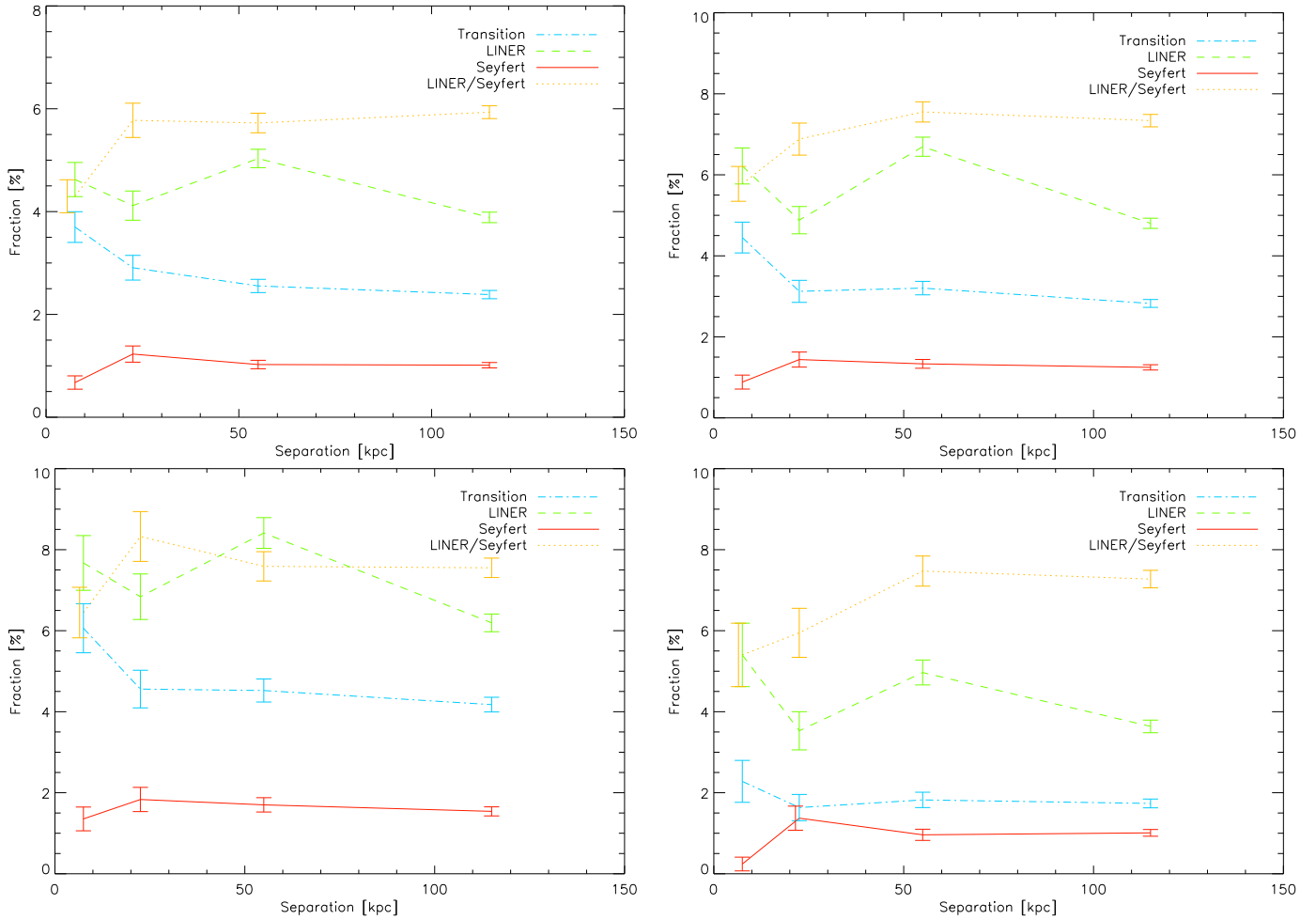


**Figure 7.** Fraction of Transition, LINER, Seyfert and LINER/Seyfert galaxies in each of the following four separation bins: 0-15kpc, 15-30kpc, 30-80kpc and 80-150kpc. Top Left: All masses and environments. Top Right: Restricted to high mass ( $M \geq 10^{10} M_{\odot}$ ) since AGN activity is unlikely in lower mass galaxies. Bottom left: High mass galaxies ( $M \geq 10^{10} M_{\odot}$ ) in field environments. Bottom right: High mass galaxies ( $M \geq 10^{10} M_{\odot}$ ) in group environments.

in emission line processes, leading to an evolution in a galaxy’s location in the BPT diagram. However, based on our BPT analysis, where Seyferts are the only category to definitely harbour AGN activity, we see little evidence that mergers are triggering AGN activity during the close pairs stage of merging. We propose that, if AGN activity is ignited in some interacting massive galaxies as theoretically predicted, this process may lead to another class of AGN activity, or take place at the post-merger stage once the merging black holes have coalesced (see Carpineti et al. 2012).

## ACKNOWLEDGEMENTS

We are grateful to the anonymous referee for many useful comments that improved the original manuscript. We thank Sara Ellison and David Patton for their helpful and constructive comments, Daniel Mortlock for his help with statistical calculations, and Mike Blanton for his publically available Kcorrect code. SK acknowledges research fellowships from the 1851 Royal Commission, Imperial College London

and Worcester College Oxford and support from the BIPAC institute at Oxford.

Funding for the SDSS and SDSS-II has been provided by the Alfred P. Sloan Foundation, the Participating Institutions, the National Science Foundation, the U.S. Department of Energy, the National Aeronautics and Space Administration, the Japanese Monbukagakusho, the Max Planck Society, and the Higher Education Funding Council for England. The SDSS Web Site is <http://www.sdss.org/>. The SDSS is managed by the Astrophysical Research Consortium for the Participating Institutions. The Participating Institutions are the American Museum of Natural History, Astrophysical Institute Potsdam, University of Basel, University of Cambridge, Case Western Reserve University, University of Chicago, Drexel University, Fermilab, the Institute for Advanced Study, the Japan Participation Group, Johns Hopkins University, the Joint Institute for Nuclear Astrophysics, the Kavli Institute for Particle Astrophysics and Cosmology, the Korean Scientist Group, the Chinese Academy of Sciences (LAMOST), Los Alamos National Laboratory, the Max-Planck-Institute for Astronomy (MPIA), the Max-Planck-Institute for Astrophysics (MPA),



New Mexico State University, Ohio State University, University of Pittsburgh, University of Portsmouth, Princeton University, the United States Naval Observatory, and the University of Washington.

GALEX is a NASA Small Explorer, launched in April 2003. We gratefully acknowledge NASA's support for construction, operation, and science analysis for the GALEX mission, developed in cooperation with the Centre National d'Etudes Spatiales of France and the Korean Ministry of Science and Technology.

## REFERENCES

- Alonso M. S., Lambas D. G., Tissera P., Coldwell G., 2005, in *Astronomical Society of the Pacific Conference Series*, Vol. 344, *The Cool Universe: Observing Cosmic Dawn*, C. Lidman & D. Alloin, ed., p. 107
- Arp H., 1966, *ApJS*, 14, 1
- Baldwin J. A., Phillips M. M., Terlevich R., 1981, *PASP*, 93, 5
- Barton E. J., Geller M. J., Kenyon S. J., 2000, *ApJ*, 530, 660
- Bell E. F., McIntosh D. H., Katz N., Weinberg M. D., 2003, *ApJS*, 149, 289
- Bianchi L., 2011, *Astrophys. Space Sci.*, 335, 51
- Blanton M. R., Roweis S., 2007, *AJ*, 133, 734
- Bournaud F., Powell L. C., Chapon D., Teyssier R., 2011, in *IAU Symposium*, Vol. 271, *IAU Symposium*, N. H. Brummell, A. S. Brun, M. S. Miesch, & Y. Ponty, ed., pp. 160–169
- Brinchmann J., Charlot S., White S. D. M., Tremonti C., Kauffmann G., Heckman T., Brinkmann J., 2004, *MNRAS*, 351, 1151
- Bundy K., Fukugita M., Ellis R. S., Targett T. A., Belli S., Kodama T., 2009, *ApJ*, 697, 1369
- Byrd G., Valtonen M., 1990, *ApJ*, 350, 89
- Calzetti D., Armus L., Bohlin R. C., Kinney A. L., Koornneef J., Storchi-Bergmann T., 2000, *ApJ*, 533, 682
- Carpinetti A., Kaviraj S., Darg D., Lintott C., Schawinski K., Shabala S., 2012, *MNRAS*, 420, 2139
- Cox T. J., Jonsson P., Somerville R. S., Primack J. R., Dekel A., 2008, *MNRAS*, 384, 386
- Darg D. W. et al., 2010, *MNRAS*, 401, 1552
- Debuhr J., Quataert E., Ma C.-P., 2011, *MNRAS*, 412, 1341
- Donas J. et al., 2007, *ApJS*, 173, 597
- Ellison S. L., Patton D. R., Simard L., McConnachie A. W., 2008, *AJ*, 135, 1877
- Ellison S. L., Patton D. R., Simard L., McConnachie A. W., Baldry I. K., Mendel J. T., 2010, *MNRAS*, 407, 1514
- Fukugita M., Ichikawa T., Gunn J. E., Doi M., Shimasaku K., Schneider D. P., 1996, *AJ*, 111, 1748
- Gunn J. E. et al., 1998, *AJ*, 116, 3040
- Hopkins P. F., Hernquist L., Cox T. J., Di Matteo T., Martini P., Robertson B., Springel V., 2005, *ApJ*, 630, 705
- Huchra J. P., Geller M. J., 1982, *ApJ*, 257, 423
- Hutchings J. B., 1987, *ApJ*, 320, 122
- Iglesias-Páramo J. et al., 2006, *ApJS*, 164, 38
- Joseph R. D., Meikle W. P. S., Robertson N. A., Wright G. S., 1984, *MNRAS*, 209, 111
- Kalfountzou E., Trichas M., Rowan-Robinson M., Clements D., Babbedge T., Seiradakis J. H., 2011, *MNRAS*, 413, 249
- Kauffmann G., Haehnelt M., 2000, *MNRAS*, 311, 576
- Kauffmann G. et al., 2003, *MNRAS*, 346, 1055
- Kauffmann G., White S. D. M., Guiderdoni B., 1993, *MNRAS*, 264, 201
- Kauffmann G., White S. D. M., Heckman T. M., Ménard B., Brinchmann J., Charlot S., Tremonti C., Brinkmann J., 2004, *MNRAS*, 353, 713
- Kaviraj S., Devriendt J. E. G., Ferreras I., Yi S. K., Silk J., 2009, *A&A*, 503, 445
- Kaviraj S. et al., 2007, *ApJS*, 173, 619
- Kennicutt, Jr. R. C., Roettiger K. A., Keel W. C., van der Hulst J. M., Hummel E., 1987, *AJ*, 93, 1011
- Kewley L. J., Groves B., Kauffmann G., Heckman T., 2006, *MNRAS*, 372, 961
- Kewley L. J., Heisler C. A., Dopita M. A., Lumsden S., 2001, *ApJS*, 132, 37
- Larson R. B., Tinsley B. M., 1978, *ApJ*, 219, 46
- Lonsdale C. J., Persson S. E., Matthews K., 1984, *ApJ*, 287, 95
- Martin D. C. et al., 2005, *ApJL*, 619, L1
- Meurer G. R., Heckman T. M., Calzetti D., 1999, *ApJ*, 521, 64
- Mihos J. C., 1995, *ApJL*, 438, L75
- Mihos J. C., Hernquist L., 1996, *ApJ*, 464, 641
- Morrissey P. et al., 2007, *ApJS*, 173, 682
- Morrissey P. et al., 2005, *ApJL*, 619, L7
- Norberg P. et al., 2002, *MNRAS*, 336, 907
- Pannella M. et al., 2009, *ApJL*, 698, L116
- Patton D. R., Ellison S. L., Simard L., McConnachie A. W., Mendel J. T., 2011, *MNRAS*, 412, 591
- Patton D. R., Grant J. K., Simard L., Pritchett C. J., Carlberg R. G., Borne K. D., 2005, *AJ*, 130, 2043
- Patton D. R. et al., 2002, *ApJ*, 565, 208
- Salim S. et al., 2005, *ApJL*, 619, L39
- Salpeter E. E., 1955, *ApJ*, 121, 161
- Sanders D. B., Mirabel I. F., 1996, *ARA&A*, 34, 749
- Sanders D. B., Soifer B. T., Elias J. H., Madore B. F., Matthews K., Neugebauer G., Scoville N. Z., 1988, *ApJ*, 325, 74
- Sarzi M. et al., 2006, *MNRAS*, 366, 1151
- Schlegel D. J., Finkbeiner D. P., Davis M., 1998, *ApJ*, 500, 525
- Simard L., Mendel J. T., Patton D. R., Ellison S. L., McConnachie A. W., 2011, *ApJS*, 196, 11
- Smith E. P., Heckman T. M., Bothun G. D., Romanishin W., Balick B., 1986, *ApJ*, 306, 64
- Soares D. S. L., 2007, *AJ*, 134, 71
- Toomre A., Toomre J., 1972, *ApJ*, 178, 623
- Trichas M. et al., 2010, *MNRAS*, 405, 2243
- Wang J. L., Xia X. Y., Mao S., Cao C., Wu H., Deng Z. G., 2006, *ApJ*, 649, 722
- Wong K. C. et al., 2011, *ApJ*, 728, 119
- Woods D. F., Geller M. J., 2007, *AJ*, 134, 527
- Yang X., Mo H. J., van den Bosch F. C., Jing Y. P., 2005, *MNRAS*, 356, 1293
- Yang X., Mo H. J., van den Bosch F. C., Pasquali A., Li C., Barden M., 2007, *ApJ*, 671, 153
- Yi S. K. et al., 2005, *ApJL*, 619, L111
- York D. G. et al., 2000, *AJ*, 120, 1579